Nonlinear Dyn (2009) 57: 533–557
DOI 10.1007/s11071-008-9406-7

ORIGINAL PAPER

Nonlinear and parametric coupled vibrations of the rotor-shaft system as fault identification symptom using stochastic methods

T. Szolc · P. Tauzowski · J. Knabel · R. Stocki

Received: 22 April 2008 / Accepted: 17 July 2008 / Published online: 12 August 2008

Abstract In the paper several stochastic methods for detection and identification of cracks in the shafts of rotating machines are proposed. All these methods are based on the Monte Carlo simulations of the rotor-shaft lateral-torsional-longitudinal vibrations mutually coupled by transverse cracks of randomly selected depths and locations on the shaft. For this purpose there is applied a structural hybrid model of a real cracked rotor-shaft. This model is characterized by a high practical reliability and great computational efficiency, so important for hundreds of thousands numerical simulations necessary to build databases used in solving the inverse problem, i.e. crack parameter identifications. In order to ensure a good identification accuracy, for creating the Monte Carlo samples of data points there are proposed special probability density functions for locations and depths of the crack. Such an approach helps in enhancing databases corresponding to the most probable faults of the rotor-shaft system of the considered rotor machine. In the presented study six different database sizes are considered to compare identification efficiency and accuracy of considered methods. A sufficiently large database enables us to estimate almost immediately (usually in less than one second) the crack parameters with precision that is in most of the cases acceptable in practice. Then, as a next stage, one of the proposed fast improvement algorithms can be applied to refine identification results in a reasonable time. The proposed methods seem to provide very convenient diagnostic tools for industrial applications.

Keywords Crack rotor dynamics · Nonlinear and parametric vibrations · Hybrid modeling · Monte Carlo simulation · Crack identification methods

1 Introduction

An efficient detection and localization of defects in the most heavily affected parts of modern turbomachinery is always a very important task in exploitation of these machines. For this purpose the on-line acting monitoring routines during regular operation of the turbomachinery are the most advantageous. Majority of the fault identification methods applied until present are based on analyses of vibratory behavior associated with rotational motion of the rotor-machine. Since natural frequencies and mode-shape functions are usually not very sensitive to local imperfections of such mechanical systems caused by relatively small defects, e.g. cracks in the rotor-shafts, the corresponding changes of these quantities cannot serve as effective fault indicators. Thus, nonlinear effects introduced

T. Szolc · P. Tauzowski · J. Knabel · R. Stocki (✉)
Institute of Fundamental Technological Research, Polish Academy of Sciences, ul. Świetokrzyska 21, 00-049 Warsaw, Poland
e-mail: rstocki@ippt.gov.pl

by the mentioned defects, e.g. due to crack breathing, have been used by some authors as fault diagnostic symptoms [1–4]. Fortunately, typical defects observed in the rotor-machines, e.g. transverse cracks in the rotor-shafts, shaft segment misalignments or bearing eccentricities, yield disturbances resulting in couplings between several kinds of vibrations affecting the rotor-shaft systems, i.e. coupling of bending vibrations with torsional and axial vibrations [3, 5, 6]. As it follows from numerous theoretical studies and practical observations, in the cases of the above-mentioned defects of the rotor-machines these couplings are usually nonlinear or parametric in character. Moreover, magnitudes of the additional vibration components induced by the coupling effects are large enough to serve efficiently as identification measure for the given kind of a defect. According to the above, in the case of cracked rotor-shafts there were studied, e.g. in [4, 7, 8], coupling effects between shaft bending and torsional vibrations regarded as crack occurrence diagnostic symptoms caused by a local anisotropy of the faulty shaft cross section. The complete coupling effects due to anisotropy of the cracked shaft cross section, i.e. between shaft bending, torsional and axial vibrations, are taken into consideration in [3, 5, 6]. The numerical simulation results of coupled vibrations of the cracked rotor-shaft systems obtained in [3, 5] by means of the one-dimensional finite element model of the real object have been qualitatively analyzed in [5] and used for composing the cause–symptom relationships necessary for crack diagnostics in [3]. Then, in order to identify crack depth and position on the shaft, several methods of inverse mapping of the on-line measured response–investigated symptom relationships have been developed. Most of them employ neural networks or other adaptive systems , see e.g. [3]. Since the fault identification routines based on the neural networks seem to be quite labor-consuming and not always sufficiently accurate, in the current paper, as an alternative approach, stochastic methods of transverse crack detection and localization in the rotating shafts are proposed.

All the proposed methods of fault identification are based on the Monte Carlo simulation of lateral–torsional–axial vibrations coupled by the crack in the rotor-shaft represented by a proper theoretical model. Here, by means of the Monte Carlo simulation, an input–output database is generated for various crack depths and locations on the rotor-shaft. The identification of the most probable crack parameters consists in analyzing the database points in the neighborhood of read-outs obtained from on-line monitoring of the real machine. The methods also provide a measure of confidence for the identified values of crack parameters. In order to guarantee that the relationship of interest is properly investigated for the most probable crack occurrence events, some assumptions concerning probability distribution functions of the random crack parameters have to be made. This is one of the major concepts of the proposed approach, which is discussed in detail in Sect. 5.

The numerical simulations should be carried out using a theoretical model which guarantees sufficiently accurate representation of the real object as well as a very high computational efficiency, so important for the Monte Carlo simulation involving computations repeated thousands or even hundreds of thousands times for various crack depths and axial positions on the shaft. For this purpose, similarly as in [6, 9], there is applied a hybrid mechanical model built in an analogous way as the beam-like finite element models commonly used for the rotor-shaft systems.

To demonstrate a high identification accuracy of this approach and its good applicability for practical engineering requirements, the computational tests have been performed for the large multi-bearing rotor-shaft system of the steam turbogenerator. The results of this study are presented in Sect. 6.

2 Assumptions for the hybrid mechanical model

In order to obtain sufficiently reliable results of numerical simulations, together with a reasonable computational efficiency, the vibrating rotor-shaft system of a rotor machine is usually modeled by means of the one-dimensional finite elements of the beam-type. Nevertheless, such models are characterized by relatively high number of degrees of freedom in the range between hundreds and even thousands. The commonly applied cracked shaft models introduce nonlinear and parametric effects into the entire dynamical system. Thus, for such large finite-element models, proper algorithms reducing number of degrees of freedom have to be employed in order to shorten computer simulation times. Moreover, for the Monte Carlo simulation performed for numerous axial fault positions along the entire rotor-shaft line, the discretization mesh density of the finite element model must be ap-

propriately modified in each case. Thus the necessary corresponding multiple reductions of degrees of freedom are troublesome and can lead to computational inaccuracies.

According to the above, in order to avoid the above-mentioned drawbacks of the finite element approach and to maintain the obvious advantages of this method, in this paper dynamic investigations of the entire rotating system are performed by means of the one-dimensional hybrid structural model consisting of continuous visco-elastic macro-elements and discrete oscillators. This model is employed here for eigenvalue analyses as well as for Monte Carlo numerical simulations of coupled nonlinear lateral–torsional–axial vibrations of the cracked rotor-shaft. Similarly as in [6, 9], in this model successive cylindrical segments of the stepped rotor-shaft are substituted by flexurally, axially and torsionally deformable cylindrical macro-elements of continuously distributed inertial visco-elastic properties. Since in the rotor-shaft system of the real rotor machine the bladed disks and gears are attached along many shaft segments by means of shrink-fit connections, the entire inertia of such fragments is increased, whereas usually the shaft cross sections only are affected by elastic deformations due to transmitted loadings. Thus, the corresponding visco-elastic macro-elements in the hybrid model must be characterized by geometric cross-sectional parameters responsible for their elastic and inertial properties and by the separate layers responsible for inertial properties only. These are the diametric and polar moments of inertia as well as the cross-sectional areas. Such exemplary ith continuous visco-elastic macro-element is presented in Fig. 1. In this figure symbols $A_{\mathrm{E}i}$, $I_{\mathrm{E}i}$ and $I_{0\mathrm{E}i}$ denote respectively the cross-sectional area, diametric and polar moments of inertia responsible for elastic properties, $i = 1, 2, \ldots, n$, where n is the total number of macro-elements in the considered hybrid model. Symbols $A_{\mathrm{I}i}$, $I_{\mathrm{I}i}$ and $I_{0\mathrm{I}i}$ denote respectively the cross-sectional area, diametric and polar moments of inertia responsible for inertial properties. Moreover, values of the material constants of each ith macro-element, i.e. Young's and Kirchhoff's moduli, can depend on the actual operation temperature of the corresponding rotor-shaft segment of the machine. The transverse and torsional external loads continuously distributed along the macro-element length l_i, if any, are described by the two-argument functions $p_i(x, t)$ and $q_i(x, t)$, where x is the spatial coordinate and t denotes time.

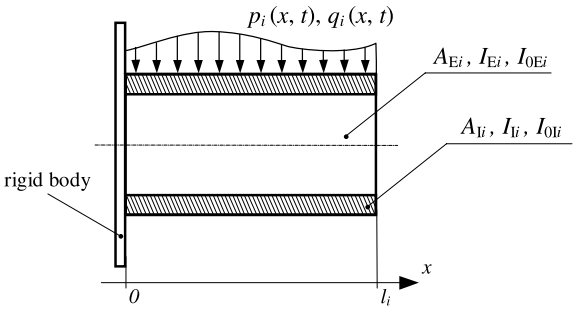

Fig. 1 Continuous visco-elastic macro-element with distinguished cross sections responsible for elastic and inertial properties

With an accuracy that is sufficient for practical purposes, in the proposed hybrid model of the rotor-shaft system, some heavy rotors or coupling disks can be represented by rigid bodies attached to the macro-element extreme cross sections, as shown in Fig. 1. Each journal bearing is represented by the use of a dynamic oscillator of two degrees of freedom, where apart from the oil-film interaction also the visco-elastic properties of the bearing housing and foundation are taken into consideration. This bearing model makes possible to represent with relatively high accuracy kinetostatic and dynamic anisotropic and anti-symmetric properties of the oil-film in the form of constant stiffness and damping coefficients, see [3]. An example of such a hybrid model of the steam turbogenerator rotor-shaft system supported on seven journal bearings is presented in Fig. 2.

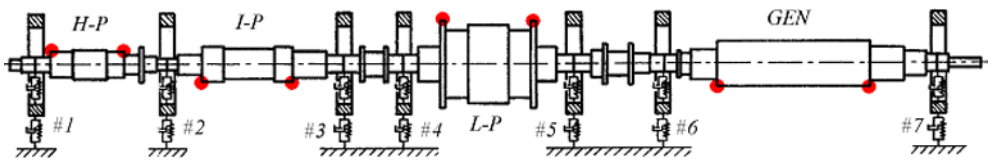

Fig. 2 Hybrid mechanical model of the steam turbogenerator rotor-shaft system

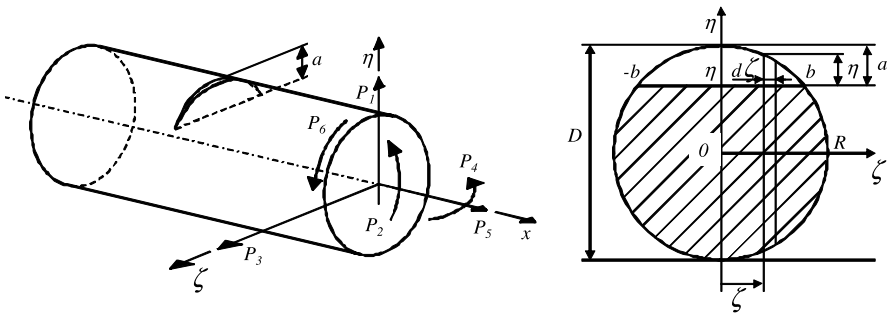

Fig. 3 Geometry of the cracked shaft segment

In this system in the selected fragment of the rotor-shaft there is considered a transverse crack implemented in the model by a proper elastic connection of the respective adjacent left- and right-hand-side parts of the faulty shaft segment. An exemplary cracked shaft segment with its geometrical dimensions is presented in Fig. 3. Additional flexural, torsional and axial flexibilities introduced by the crack into the shaft are represented here by means of mass-less springs connecting the adjacent beam macro-elements substituting cracked shaft segment. Stiffness values of these springs are determined according to [3, 5, 7] using the fundamentals of fracture mechanics.

In this study, a hinge model of the transverse crack has been applied. Thus, the coefficients of the above-mentioned additional flexural, torsional and axial flexibilities introduced by the crack are determined using the Paris equation based on the Castigliano theorem. In the considered case a double-partial differentiation of the strain energy density function with respect to the virtual generalized loadings yields the coefficients of additional flexibility caused by the crack:

$$f_{ij} = \frac{\partial^2}{\partial P_i \partial P_j} \int_{-b}^{b} \int_{0}^{a} J(\eta)\, \mathrm{d}\eta\, \mathrm{d}\zeta = f_{ij}(a, D, E, \nu), \quad i, j = 1, 2, \ldots, 6, \tag{1}$$

where P_i, P_j are the virtual generalized loadings acting on the cracked shaft segment of diameter D, as shown in Fig. 3; a denotes the crack depth, E is Young's modulus, ν denotes Poisson's ratio of the shaft material and $b = \sqrt{a(D-a)}$. Symbol $J(\eta)$ in (1) is the strain-energy density function

$$J(\eta) = \frac{1}{E(1-\nu^2)} \left\{ \left[\sum_{i=1}^{6} K_{\mathrm{I}i}(P_i, \eta, D) \right]^2 + \left[\sum_{i=1}^{6} K_{\mathrm{II}i}(P_i, \eta, D) \right]^2 + (1+\nu) \left[\sum_{i=1}^{6} K_{\mathrm{III}i}(P_i, \eta, D) \right]^2 \right\}, \tag{2}$$

where $K_{\mathrm{I}i}, K_{\mathrm{II}i}, K_{\mathrm{III}i}$ denote the stress intensity factors of the first, second and third mode, respectively. Exact analytical expressions for the strain density function for the cracked shafts can by found, e.g., in [3, 5, 7]. As it follows from these papers, since the stress intensity factors $K_{\mathrm{I}i}, K_{\mathrm{II}i}, K_{\mathrm{III}i}$ are quadratic functions of the virtual generalized loadings P_i, the coefficients of flexibility obtained using (1) are functions of the material constants and cracked shaft cross-sectional parameters a and D. These coefficients create the 6×6 symmetrical local-flexibility matrix. The inverse of this matrix becomes the crack local-stiffness-coefficients matrix of the following form:

$$\begin{bmatrix} c_{11} & 0 & c_{13} & 0 & 0 & c_{16} \\ 0 & c_{22} & 0 & c_{24} & c_{25} & 0 \\ c_{13} & 0 & c_{33} & 0 & 0 & c_{36} \\ 0 & c_{24} & 0 & c_{44} & c_{45} & 0 \\ 0 & c_{25} & 0 & c_{45} & c_{55} & 0 \\ c_{16} & 0 & c_{36} & 0 & 0 & c_{66} \end{bmatrix}. \tag{3}$$

The above matrix is not diagonal. If we assume, according to Fig. 3, that the direction "1" corresponds to translational motion along 0η axis, the direction "2" corresponds to rotational motion around 0ζ axis, the direction "3" corresponds to translational motion along 0ζ axis, the direction "4" corresponds to rotational motion around 0η axis, the direction "5" corresponds to translational motion along the shaft rota-

tion axis $0x$ and the direction "6" corresponds to rotational motion around $0x$ axis, it follows from (3) that due to local cross-sectional anisotropy caused by the crack the shaft transverse motion is directly coupled with its rotational motion around the rotation axis, as well as the rotational motions around diameters are directly coupled with translational motions in the axial direction. According to the above, such a crack model makes possible to take into consideration coupling effects between the torsional and axial vibrations of the rotor-shaft with its bending vibrations induced by residual unbalances of the rotating system.

All coefficients in the local-stiffness matrix (3) remain constant in the coordinate system $\{0x\eta\zeta\}$ rotating with the shaft. Since the further considerations are going to be carried out in an inertial non-rotating coordinate system, matrix (3) has to be properly transformed and then all stiffness coefficients become time-dependent functions

$$
\begin{aligned}
k^*_{11}(t) &= \frac{1}{2}(c_{11}+c_{33}) + \frac{1}{2}(c_{11}-c_{33})\cos(2\alpha) \\
&\quad - c_{13}\sin(2\alpha), \\
k^*_{13}(t) &= \frac{1}{2}(c_{11}-c_{33})\sin(2\alpha) + c_{13}\cos(2\alpha), \\
k^*_{16}(t) &= c_{16}\cos(\alpha) - c_{36}\sin(\alpha), \\
k^*_{33}(t) &= \frac{1}{2}(c_{11}+c_{33}) - \frac{1}{2}(c_{11}-c_{33})\cos(2\alpha) \\
&\quad + c_{13}\sin(2\alpha), \\
k^*_{36}(t) &= c_{16}\sin(\alpha) + c_{36}\cos(\alpha), \\
k^*_{22}(t) &= \frac{1}{2}(c_{22}+c_{44}) + \frac{1}{2}(c_{22}-c_{44})\cos(2\alpha) \\
&\quad - c_{24}\sin(2\alpha), \\
k^*_{24}(t) &= \frac{1}{2}(c_{22}-c_{44})\sin(2\alpha) + c_{24}\cos(2\alpha), \\
k^*_{25}(t) &= c_{25}\cos(\alpha) - c_{45}\sin(\alpha), \\
k^*_{44}(t) &= \frac{1}{2}(c_{22}+c_{44}) - \frac{1}{2}(c_{22}-c_{44})\cos(2\alpha) \\
&\quad + c_{24}\sin(2\alpha), \\
k^*_{45}(t) &= c_{25}\sin(\alpha) + c_{45}\cos(\alpha), \\
k^*_{55}(t) &= c_{55}, \\
k^*_{66}(t) &= c_{66},
\end{aligned}
\tag{4}
$$

where $\alpha = \Omega t + \alpha_p$, Ω being the shaft constant angular speed and α_p the angle of crack circumferential position on the shaft with respect of the vector of resultant excitation caused by the shaft residual unbalance.

3 Mathematical formulation of the cracked rotor-shaft vibration problem

In the hybrid model, motion of cross sections of each visco-elastic macro-element of the length l_i is governed by the partial differential equations derived using the Timoshenko and Rayleigh rotating beam theory for flexural motion as well as by the hyperbolic equations of the wave type, separately for torsional and axial motion. Similarly as in [6, 9], mutual connections of the successive macro-elements creating the stepped shaft as well as their interactions with the supports and rigid bodies representing the heavy rotors are described by equations of boundary conditions. These equations contain geometrical conditions of conformity for translational and rotational displacements of extreme cross sections $x = L_i = l_1 + l_2 + \cdots + l_{i-1}$ of the adjacent $(i-1)$th and the ith elastic macro-elements:

$$
\begin{aligned}
&v_{i-1}(x,t) = v_i(x,t), \quad \frac{\partial v_{i-1}(x,t)}{\partial x} = \frac{\partial v_i(x,t)}{\partial x}, \\
&\theta_{i-1}(x,t) = \theta_i(x,t), \quad z_{i-1}(x,t) = z_i(x,t),
\end{aligned}
\tag{5}
$$

where $v_i(x,t) = u_i(x,t) + j w_i(x,t)$, $u_i(x,t)$ being the lateral displacement in the vertical direction and $w_i(x,t)$ the lateral displacement in the horizontal direction, j the imaginary number; $\theta_i(x,t)$ is the angular displacement with respect to the shaft rotational uniform motion with the constant velocity Ω, and $z_i(x,t)$ the translational axial displacement; $i = 1, 2, \ldots, n$ and n the total number of macro-elements in the hybrid model.

The second group of boundary conditions are dynamic ones, which contain linear, nonlinear and parametric equations of equilibrium for external forces and torques, static and dynamic unbalance forces and moments, inertial, elastic and external damping forces,

support reactions and gyroscopic moments. For example, the dynamic boundary conditions formulated for the rotating Rayleigh beam, and describing a simple connection of the mentioned adjacent $(i-1)$th and the ith elastic macro-elements, have the following form:

$$\begin{aligned}
&E_i I_{\mathrm{E}i}\frac{\partial^3 v_i}{\partial x^3} - \rho I_{\mathrm{I}i}\frac{\partial^3 v_i}{\partial x \partial t^2} - E_{i-1} I_{\mathrm{E},i-1}\frac{\partial^3 v_{i-1}}{\partial x^3} \\
&\quad + \rho I_{\mathrm{I},i-1}\frac{\partial^3 v_{i-1}}{\partial x \partial t^2} + j\Omega\rho I_{0\mathrm{I}i}\frac{\partial^2 v_i}{\partial x \partial t} \\
&\quad - j\Omega\rho I_{0\mathrm{I},i-1}\frac{\partial^2 v_{i-1}}{\partial x \partial t} = 0, \\
&E_i I_{\mathrm{E}i}\frac{\partial^2 v_i}{\partial x^2} - E_{i-1} I_{\mathrm{E},i-1}\frac{\partial^2 v_{i-1}}{\partial x^2} = 0, \\
&G_i I_{0\mathrm{E}i}\frac{\partial \theta_i}{\partial x} - G_{i-1} I_{0\mathrm{E},i-1}\frac{\partial \theta_{i-1}}{\partial x} = 0, \\
&E_i A_{\mathrm{E}i}\frac{\partial z_i}{\partial x} - E_{i-1} A_{\mathrm{E},i-1}\frac{\partial z_{i-1}}{\partial x} = 0,
\end{aligned} \tag{6}$$

where $E_i = E_i(T_i), G_i = G_i(T_i)$ denote respectively Young's and Kirchhoff's moduli of the shaft material of the density ρ, which are expressed as functions of the actual operation temperature T_i of the ith macro-element corresponding to the given rotor-shaft segment of the machine.

The transverse crack in the given shaft segment is also described by boundary conditions formulated for extreme cross sections of the corresponding $(k-1)$th and kth adjacent macro-elements representing this shaft segment. Then, their dynamic equations of equilibrium of forces and moments (6) remain valid. However, the geometric equations of displacement conformity (5) must be appropriately substituted by properly modified relations. If in the shaft the transverse crack is assumed, its "breathing" process usually has to be taken into consideration as, e.g., in [2, 5, 6]. Then, for the "open" crack in the shaft cross section $x = L_{cr} = l_1 + l_2 + \cdots + l_{k-1}$, the respective boundary conditions have the following form:

$$\begin{aligned}
&E_{k-1} I_{\mathrm{E},k-1}\frac{\partial^3 v_{k-1}}{\partial x^3} \\
&\quad = \big(k^*_{11}(t) + jk^*_{13}(t)\big)\mathrm{Re}[v_k - v_{k-1}] \\
&\qquad + j\big(k^*_{33}(t) - jk^*_{13}(t)\big)\,\mathrm{Im}[v_k - v_{k-1}] \\
&\qquad + \big(k^*_{16}(t) + jk^*_{36}(t)\big)[\theta_k - \theta_{k-1}], \\
&E_{k-1} I_{\mathrm{E},k-1}\frac{\partial^2 v_{k-1}}{\partial x^2} \\
&\quad = \big(k^*_{22}(t) + jk^*_{24}(t)\big)\mathrm{Re}\left[\frac{\partial v_k}{\partial x} - \frac{\partial v_{k-1}}{\partial x}\right] \\
&\qquad + j\big(k^*_{44}(t) - jk^*_{24}(t)\big)\,\mathrm{Im}\left[\frac{\partial v_k}{\partial x} - \frac{\partial v_{k-1}}{\partial x}\right] \\
&\qquad + \big(k^*_{25}(t) + jk^*_{45}(t)\big)[z_k - z_{k-1}], \\
&G_{k-1} I_{0\mathrm{E},k-1}\frac{\partial \theta_{k-1}}{\partial x} \\
&\quad = c_{66}[\theta_k - \theta_{k-1}] + k^*_{16}(t)\mathrm{Re}[v_k - v_{k-1}] \\
&\qquad + k^*_{36}(t)\,\mathrm{Im}[v_k - v_{k-1}], \\
&E_{k-1} A_{\mathrm{E},k-1}\frac{\partial z_{k-1}}{\partial x} \\
&\quad = c_{55}[z_k - z_{k-1}] + k^*_{25}(t)\mathrm{Re}\left[\frac{\partial v_k}{\partial x} - \frac{\partial v_{k-1}}{\partial x}\right] \\
&\qquad + k^*_{45}(t)\,\mathrm{Im}\left[\frac{\partial v_k}{\partial x} - \frac{\partial v_{k-1}}{\partial x}\right],
\end{aligned} \tag{7}$$

where the local-stiffness coefficients $c_{55}, c_{66}, k^*_{ij}(t)$, $i, j = 1, 2, \ldots, 6$, are defined in (1) and (3).

The open/closed-criterion of crack "breathing" can be described by the following relation formulated in the coordinate system rotating with the shaft:

$$\begin{aligned}
&\Delta\varphi_k(L_{cr}, t) > 0, \quad \text{i.e. the crack is open, and} \\
&\Delta\varphi_k(L_{cr}, t) \leqslant 0, \quad \text{i.e. the crack is closed,}
\end{aligned} \tag{8}$$

where:

$$\begin{aligned}
&\Delta\varphi_k(L_{cr}, t) \\
&\quad = \left(\frac{\partial u_k(x,t)}{\partial x} - \frac{\partial u_{k-1}(x,t)}{\partial x}\right)\cdot\cos(\alpha) \\
&\qquad + \left(\frac{\partial w_k(x,t)}{\partial x} - \frac{\partial w_{k-1}(x,t)}{\partial x}\right)\cdot\sin(\alpha)
\end{aligned}$$

for $x = L_{cr}$.

It is assumed that for the "closed" crack, i.e. for (8_2), the geometric boundary conditions (5) are valid instead of relations (7). Moreover, if the crack is closed and the shaft cracked vicinity is compressed due to the axial vibrations, the boundary condition (5_4) is valid. However, for the vicinity of the cracked shaft in tension this relation must be substituted by (7_4).

It should be noticed here that the problem of cracked shaft is formulated as a parametric-nonlinear one, because the considered system changes its configuration depending on whether the crack is temporarily "open" or "closed" [6]. The above equations of the boundary conditions ($6_{1,2}$) and ($7_{1,2}$) are formulated using the Rayleigh beam theory. In an analogous way, such boundary conditions are derived in the framework of the Timoshenko beam theory.

It is worth to mention that similar approach for crack modeling has been applied in [3, 5] for one-dimensional shaft representation using the finite element method. In those cases the local shaft weakening due to a transverse crack is artificially distributed along the entire beam finite element corresponding to the faulty shaft segment by a proper modification of its local-stiffness matrix. However, as mentioned above, in the hybrid model used in this work the crack is implemented in the form of a discrete mutual connection of two continuous parts of the cracked shaft segment, which is represented by the visco-elastic macro-elements with numbers $k-1$ and k. Such an approach seems to represent better a local character of shaft weakening by the crack.

In order to perform simulation of forced vibrations of the rotor-shafts taking into consideration the hinge model of crack breathing, it is necessary to determine two separate sets of orthogonal eigenfunctions: for the cracked and uncracked system. Relations (7) demonstrate, how the crack couples the rotor-shaft bending vibrations with the torsional and axial vibrations. All coupling terms in (7) are parametric because they contain the explicit time-variable stiffness coefficients $k^*_{11}(t), k^*_{13}(t)$, $k^*_{33}(t), k^*_{16}(t)$, $k^*_{36}(t), k^*_{22}(t)$, $k^*_{24}(t)$, $k^*_{25}(t)$, $k^*_{44}(t)$ and $k^*_{45}(t)$ defined by relations (4). As it follows from (3) and (4), $k^*_{11}(t), k^*_{13}(t)$, $k^*_{33}(t)$, $k^*_{22}(t)$, $k^*_{24}(t)$ and $k^*_{44}(t)$ are responsible for the mutual bending-to-bending cross-coupling in two perpendicular planes in the above-mentioned inertial non-rotating coordinate system. Apart from the terms in (4) oscillating around zero-mean value with single- 1X and double-synchronous 2X frequencies of the rotating shaft, $k^*_{11}(t), k^*_{33}(t), k^*_{22}(t)$ and $k^*_{44}(t)$ contain also constant average components. However, the variable stiffness coefficients in the terms which couple the bending vibrations with torsional ones, i.e. $k^*_{16}(t)$ and $k^*_{36}(t)$, as well as the stiffness coefficients in the terms which couple the bending vibrations with axial vibrations, i.e. $k^*_{25}(t)$ and $k^*_{45}(t)$, are characterized by the components fluctuating around zero-mean value with only single-synchronous 1X frequency of the rotating shaft. In order to perform an analysis of natural elastic vibrations, all the forcing, viscous, parametric and unbalance terms in the boundary conditions have been omitted. Due to the truncation of these terms, it follows from (7) that the bending, torsional and axial vibrations of the rotor-shaft system are mutually uncoupled. According to the above, similarly as in the case of the uncracked system, the elastic bending, torsional and axial eigenvalue problems for the rotor-shaft with a crack can be solved separately. Thus, in both cases one obtains separate characteristic equations for the considered three eigenvalue problems. These are:

$$\begin{aligned} &\mathbf{A}(\omega)\mathbf{B}=\mathbf{0}, && \text{for the rotor-shaft bending vibrations,}\\ &\mathbf{C}(\omega)\mathbf{D}=\mathbf{0}, && \text{for the rotor-shaft torsional vibrations,}\\ &\mathbf{E}(\omega)\mathbf{F}=\mathbf{0}, && \text{for the rotor-shaft axial vibrations,} \end{aligned} \tag{9}$$

where $\mathbf{A}(\omega)$ is the complex characteristic matrix and $\mathbf{C}(\omega), \mathbf{E}(\omega)$ are the real characteristic matrices, and $\mathbf{B}, \mathbf{D}, \mathbf{F}$ denote the vectors of unknown constant coefficients in the analytical eigenfuctions defined in [6, 7, 9] for each macro-element in the hybrid model. Thus, the determination of natural frequencies reduces to the search for values of ω, for which the characteristic determinants of matrices $\mathbf{A}, \mathbf{C}$ and $\mathbf{E}$ are equal to zero. The bending, torsional and axial eigenmode functions are then obtained by solving respective equations (9).

According to the described above approach, in comparison with the corresponding uncracked rotor-shaft, the eigenmodes obtained for the cracked system are characterized by a local weakening caused by this crack. This weakening is expressed by the constant stiffness coefficients c_{55} and c_{66} in (4) and (7), respectively, for the axial and torsional eigenmodes as well as by the average stiffness coefficients $0.5(c_{11}+c_{33})$ and $0.5(c_{22}+c_{44})$ in (4) in the non-rotating inertial coordinate system for the bending eigenmodes. Moreover, as it follows from (7), the bending eigenmodes become mutually cross-coupled by the crack in the two perpendicular planes.

According to the above, the coupling effects between the bending, torsional and axial vibrations are of a purely oscillatory character in the non-rotating inertial coordinates. Thus, all parametric terms in (7) temporarily neglected for the eigenvalue problem solution

are going to be used for the forced vibration analysis in order to simulate bending, torsional and axial vibrations as mutually coupled by the crack.

The solution for the forced vibration analysis has been obtained using the analytical–computational approach demonstrated in detail in [9]. Solving the differential eigenvalue problem for the linearized orthogonal system and an application of the Fourier solutions in the form of series leads to the set of modal equations in the Lagrange coordinates

$$\mathbf{M}(\Omega t)\ddot{\mathbf{r}}(t) + \mathbf{C}(\Omega, \Omega t)\dot{\mathbf{r}}(t) + \mathbf{K}\big(\Delta\varphi(t), \Omega t\big)\mathbf{r}(t) = \mathbf{F}\big(t, \Omega^2, \Omega t\big), \tag{10}$$

where:

$$\mathbf{M}(\Omega t) = \mathbf{M}_0 + \mathbf{M}_u(\Omega t),$$

$$\mathbf{C}(\Omega, \Omega t) = \mathbf{C}_0 + \mathbf{C}_g(\Omega) + \boldsymbol{C}_u(\Omega t),$$

$$\mathbf{K}\big(\Delta\varphi(t), \Omega t\big) = \mathbf{K}_0 + \mathbf{K}_b + \mathbf{K}_{cr}\big(\Delta\varphi_k(L_{cr}, t), \Omega t\big).$$

The symbols $\mathbf{M}_0, \mathbf{K}_0$ denote, respectively, the constant diagonal modal mass and stiffness matrices, $\mathbf{C}_0$ is the constant symmetrical damping matrix and $\mathbf{C}_g(\Omega)$ denotes the skew symmetrical matrix of gyroscopic effects. The terms of the unbalanced effects are contained in the symmetrical matrix $\mathbf{M}_u(\Omega t)$ and in the non-symmetrical matrix $\mathbf{C}_u(\Omega t)$. Anti-symmetric elastic properties of the journal bearings are described by the skew-symmetrical matrix $\mathbf{K}_b$. Nonlinear and parametric properties of the breathing crack are described by the symmetrical matrix $\mathbf{K}_{cr}(\Delta\varphi_k(L_{cr}, t), \Omega t)$ of periodically variable coefficients, and the symbol $\mathbf{F}(t, \Omega^2, \Omega t)$ denotes the external excitation vector, e.g., due to the unbalance and gravitational forces. The Lagrange coordinate vector $\mathbf{r}(t)$ consists of subvectors of the unknown time functions in the Fourier solutions. In order to obtain the system's dynamic response, (10) are solved by means of a direct integration. The number of equations in (10) corresponds to the number of eigenmodes taken into consideration, because the forced bending, torsional and axial vibrations of the rotor-shaft are mutually coupled and thus, the total number of equations to solve is a sum of all bending, torsional and axial eigenmodes of the rotor-shaft model in the range of frequency of interest. These equations are mutually coupled by the parametric and anti-symmetrical terms regarded as external excitations expanded in series in the base of orthogonal analytical eigenfunctions. A fast convergence of the applied Fourier solutions enables us to reduce the appropriate number of the modal equations to solve, in order to obtain a sufficient accuracy of results in the given range of frequency. Here, it is necessary to solve only 15÷60 coupled modal equations (10), even in cases of great and complex mechanical systems, contrary to the classical one-dimensional beam finite element formulation leading usually to large numbers of motion equations corresponding each to more than one hundred or many hundreds degrees of freedom (if the artificial and often error-prone model reduction algorithms are not applied). However, the proposed hybrid modeling assures at least the same or even better representation of real objects as well as its mathematical description, is formally strict, demonstrates clearly the qualitative system properties and is much more convenient for a stable and efficient numerical simulation.

In the considered case of nonlinear-parametric problem, during simulations of forced vibrations, condition (8) describing the open/closed-stage of crack "breathing" is computationally predicted after each integration step by means of the *explicit* numerical method. Thus, criterion (8) indicates the actual base of eigenfunctions, in which the coupled dynamic response should be sought, i.e. the eigenfunctions corresponding respectively to the cracked or uncracked rotor-shaft line. Then, at each "switch" from the open-crack-stage into the closed-crack-stage and *vice versa*, the current system response becomes the initial condition for the "new" stage. Here, for a sufficiently small direct integration step, equal to 1/50 of the period corresponding to the upper limit of the frequency band considered, using the Newmark method almost no corrections of the time-step value were required in order to obtain sufficient accuracy of the computational routine.

4 Numerical example of vibration analysis of the cracked rotor-shaft system

The presented methodology of vibration analysis is shown here in an example of a rotor-shaft system of the typical 200 MW steam turbogenerator consisting of the single high- (HP), intermediate- (IP) and low-pressure (LP) turbines as well as of the generator-rotor (GEN). This rotor-shaft system is supported by seven

Table 1 The first 12 bending natural frequencies of the steam turbogenerator rotor-shaft system obtained by means of Rayleigh's and Timoshenko's beam theory

Eigen-form number	Natural frequency obtained using Rayleigh's beam theory [Hz]	Natural frequency obtained using Timoshenko's beam theory [Hz]	Relative difference [%]
1	22.742	22.154	−2.65
2	24.516	23.772	−3.13
3	30.924	30.707	−0.71
4	38.976	38.480	−1.29
5	45.886	45.067	−1.82
6	46.486	45.761	−1.58
7	54.183	52.741	−2.73
8	68.251	67.022	−1.83
9	107.794	105.523	−2.15
10	114.205	112.395	−1.61
11	127.162	125.468	−1.35
12	145.211	141.837	−2.38

journal bearings, as shown in Fig. 2. With the aim of theoretical study, the stepped-rotor shaft of this turbogenerator of the total length of 25.9 m has been modeled by means of $n = 49$ continuous macro-elements, as an initial approximation of its geometry. More accurate modeling of such rotor-shaft systems by means of a greater number n of macro-elements does not introduce more detrimental computational efforts. All geometrical parameters of the successive real rotor-shaft segments as well as their material constants have been determined using the detailed technical documentation of this turbogenerator. The average stiffness and damping coefficients of the oil-film in the bearings as well as the equivalent masses and stiffness and damping coefficients of the bearing housings are obtained by means of measurements and identification performed on the real object. The numerical values of Young's and Kirchhoff's moduli as the actual temperature functions $E_i(T_i)$ and $G_i(T_i)$, $i = 1, 2, \ldots, 49$, have been determined by the use of the following relationships:

$$G_i(T_i) = \frac{E_i(T_i)}{2(1+\nu)}, \quad \nu = 0.32,$$

where:

$$E_i(T_i) = \left(-0.064286(T_i - 20) + 211\right) \times 10^9 \,[\text{Pa}], \quad \text{for } T_i \leqslant 300\,[^\circ\text{C}],$$

$$E_i(T_i) = \left(-0.10(T_i - 300) + 193\right) \times 10^9 \,[\text{Pa}], \quad \text{for } 300 < T_i \leqslant 400\,[^\circ\text{C}],$$

$$E_i(T_i) = \left(-0.15(T_i - 400) + 183\right) \times 10^9 \,[\text{Pa}], \quad \text{for } 400 < T_i \leqslant 500\,[^\circ\text{C}],$$

$$E_i(T_i) = \left(-0.22(T_i - 500) + 168\right) \times 10^9 \,[\text{Pa}], \quad \text{for } T_i > 500\,[^\circ\text{C}].$$

Table 1 contains first 12 bending eigenfrequencies of the considered uncracked rotor-shaft system obtained using Rayleigh's and Timoshenko's beam rotating with the nominal rotational speed 3000 rpm. As it follows from the performed comparison, the shear effect taken into consideration in the case of Timoshenko's beam theory results in a little bit smaller natural frequency values than these determined by means of Rayleigh's beam model. Here, in the frequency range 0÷150 Hz, which is the most important from the engineering viewpoint, the respective differences slightly exceed 3%. The eigenfunctions corresponding to these natural frequencies and determined using both beam theories respectively overlay each other. According to the above, one can conclude that in this frequency range an application of Rayleigh's rotating beam theory seems to be sufficiently accurate for further simulations of forced vibrations.

The first 10 bending eigenforms corresponding to the above-mentioned natural frequencies are depicted

in Fig. 4, where the vertical projections of the bending eigenfunctions are presented by the solid lines and their horizontal projections by the dashed lines. In these plots the vertical bars illustrate the modal transverse vertical and horizontal displacement components of the rigid bodies representing the bearing housings. It is to remark that due to strong anisotropy and skew-symmetry of the journal bearing elastic properties the shapes of the eigenform vertical projections are different from the shapes of their horizontal projections, which indicates a spatial character of these eigenfunctions. As it was easy to expect, from analogous computations performed for the cracked turbogenerator rotor-shaft it follows that for the considered crack-depth values the respective differences of natural frequencies obtained for the cracked and uncracked system do not exceed 1 Hz for various axial crack positions within the frequency range $0 \div 700$ Hz. The local "un-smoothnesses" of the corresponding eigenfunctions caused by the cracks are almost unremarkable.

The first five torsional eigenfunctions together with their natural frequency values, as well as the first five axial eigenfunctions with the corresponding natural frequencies, are presented in Fig. 5. It is to remark that the 1st axial eigenform is almost of the typical rigid mode type. The corresponding natural frequency value $f_{1A} = 19.623$ Hz depends first of all on the longitudinal stiffness of bearing #5 (see Fig. 2), playing here also the thrust-bearing role. Similarly as in the case of bending eigenvibrations, all the torsional and axial eigenfunctions determined for the cracked and uncracked rotor-shaft, respectively, almost overlay each other within the investigated frequency range $0 \div 700$ Hz. Torsional natural vibrations are the most sensitive to the transverse crack, for which the greatest difference of the eigenfrequencies obtained for the cracked and uncracked shaft reach 2.5 Hz. The analogous difference of the axial natural frequencies did not exceed 0.1 Hz in the mentioned frequency range. This result confirms the known fact that values of natural frequencies and the corresponding eigenfunctions are not very sensitive to relatively small transverse cracks in fundamental components of majority of mechanical systems and structures. Thus, proper identification methods must be employed in order to detect and localize them effectively.

For this system the Monte Carlo simulation of coupled forced vibrations is performed for various crack-depth ratios in the range $a/D = 0.1 \div 0.4$ and for various axial positions on the entire length of the shaft. The system dynamic responses are obtained for the constant nominal rotational speed 3000 rpm for various circumferential crack positions α_p on the shaft within $0° \div 360°$. In addition to the static gravitational load, the only assumed source of dynamic external excitation are static residual unbalances of the high-pressure rotor equal to 90 gm each and mutually shifted "in-phase," of the intermediate-pressure rotor equal to 135 gm each, mutually shifted "in-phase" and by the phase angle $\Delta = 180°$ with respect to the unbalance of the high-pressure rotor, of the low-pressure rotor equal to 180 gm each, mutually shifted "in-phase" and "in-phase" with respect to the unbalance of the high-pressure rotor as well as of the generator-rotor equal to 270 gm each, mutually shifted "in-phase" and by the phase angle $\Delta = 180°$ with respect to the unbalance of the high-pressure rotor. This residual unbalance of the considered rotor-shaft system has been symbolically marked in Fig. 2 by the circles. Thus, the torsional and axial vibrations can be regarded here as an output effect caused by bending vibrations of the rotor-shaft line. For the assumed hybrid model of the investigated turbogenerator rotor-shaft system in the frequency range $0 \div 650$ Hz, 43 bending, 10 torsional and 7 axial eigenmodes have been considered to solve (10) with very high computational accuracy of the obtained results.

The quantities that are of particular interest for the purpose of crack identification are the ones which in regular exploitation conditions can be relatively easily measured on-line. These are lateral vibration displacements of the shaft at the bearing locations, fluctuation of shaft rotational speed due to torsional vibrations also at the bearing locations as well as the longitudinal displacements of the shaft at the shaft's both free ends and at the thrust-bearing location.

For the assumed sources of external excitations the lateral response of the considered uncracked rotor-shaft system is harmonic in character with the only one synchronous frequency component 1X. Here, the very weak torsional–lateral coupling due to the residual unbalances results in negligible torsional response and a lack of the lateral–axial coupling yields zero axial response. In the framework of the carried out Monte Carlo simulation the transverse cracks of various depths and axial locations along the entire length of the considered turbogenerator rotor-shaft line have

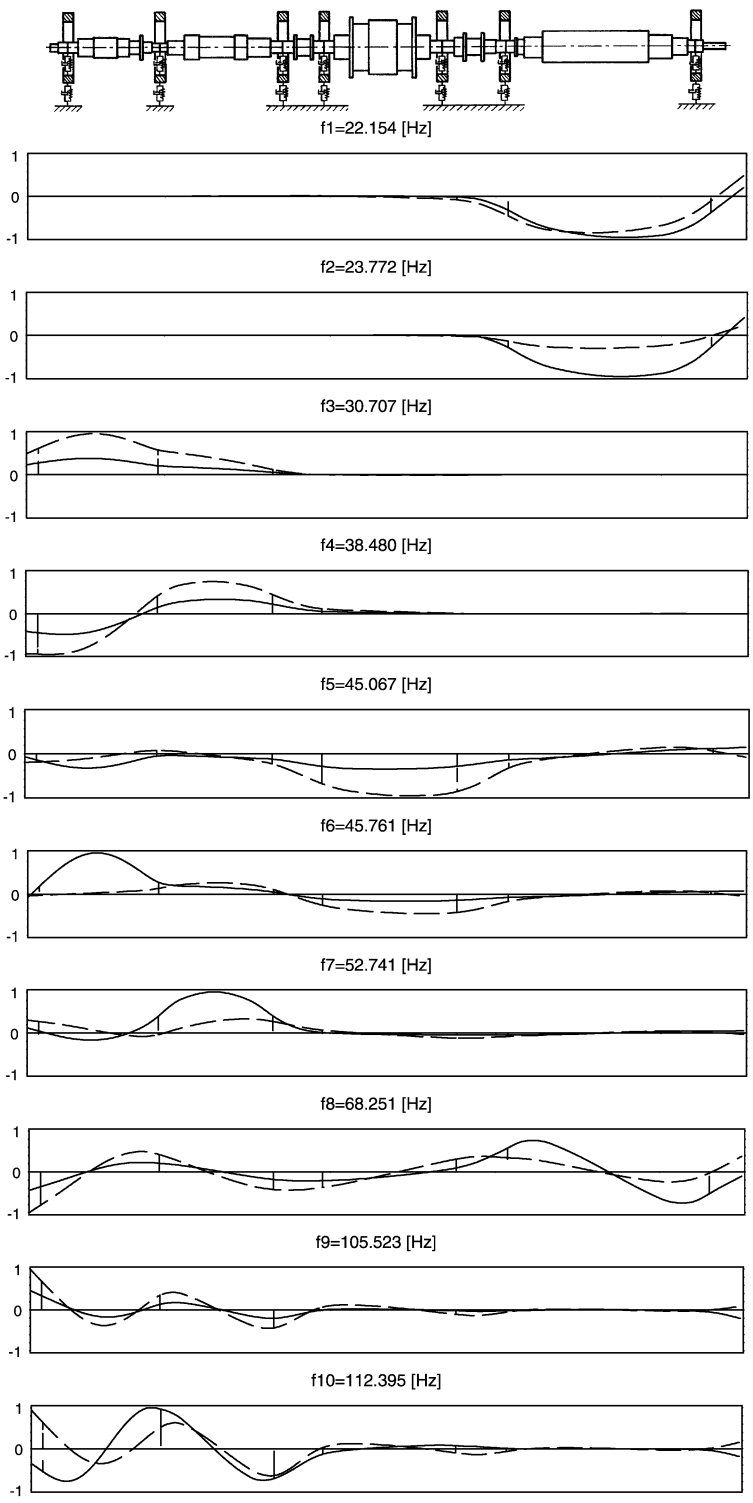

Fig. 4 Bending eigenfunctions of the hybrid model of the steam turbogenerator rotor-shaft system

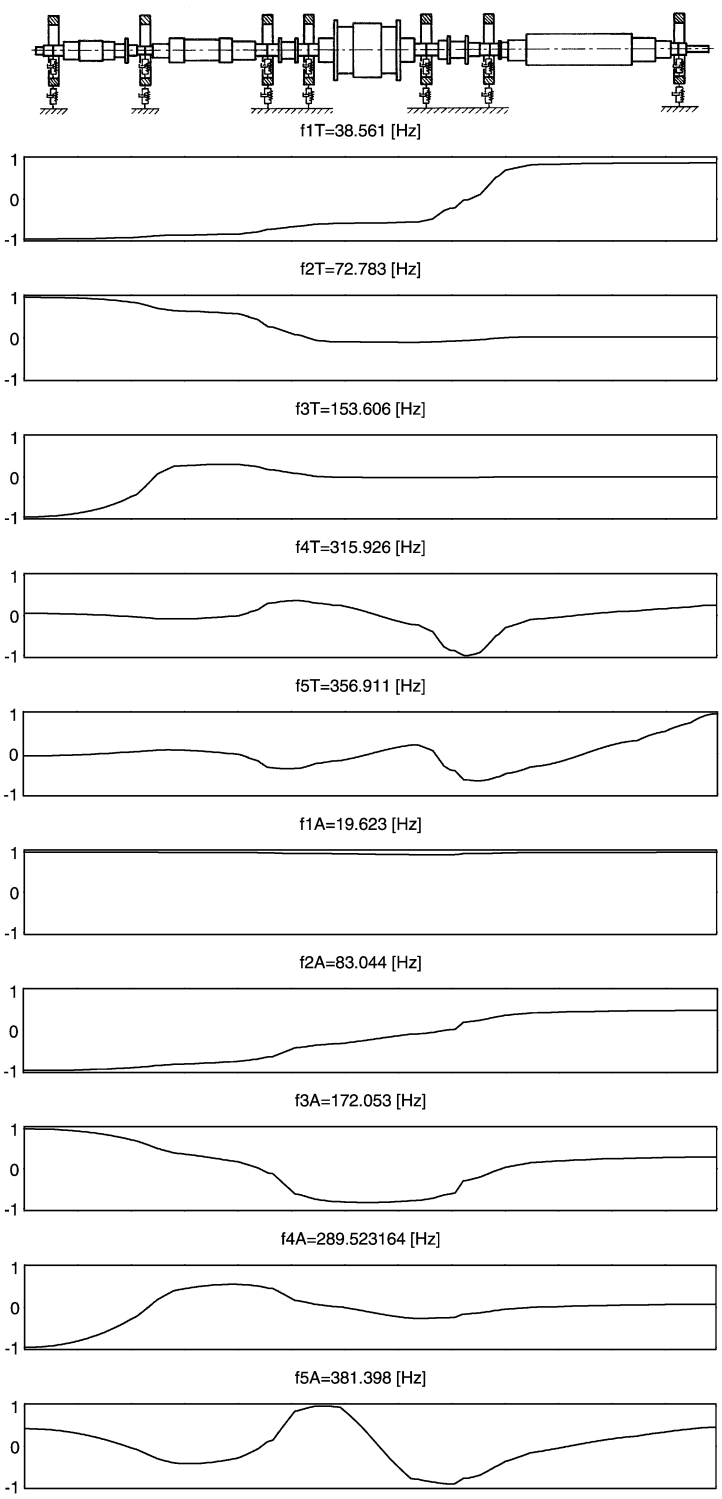

Fig. 5 Torsional and axial eigenfunctions of the hybrid model of the steam turbogenerator rotor-shaft system

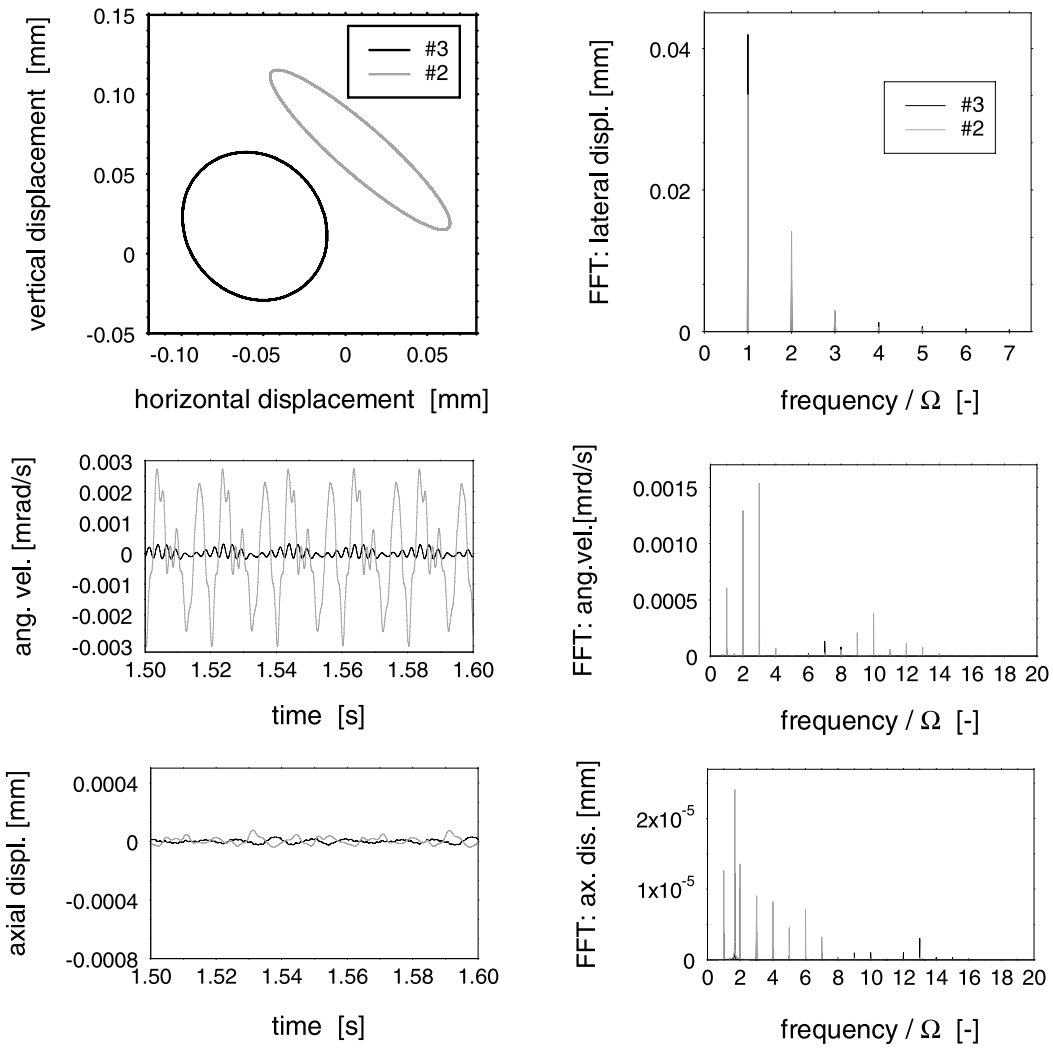

Fig. 6 Coupled dynamic response for the rotor-shaft system with the crack of the depth ratio $a/D = 0.2$ located in the intermediate-pressure rotor, close to bearing #3

been assumed. As it follows from results of these computations, the strongest influence of the crack on the system-coupled dynamic response is usually observed in the cases of investigated quantities registered in the vicinity of the given crack, i.e. close to the adjacent bearings or to the corresponding rotor-shaft ends. Figure 6 shows the plots of the coupled lateral–torsional–axial response of the system with a crack of the depth ratio $a/D = 0.2$ localized in the intermediate-pressure rotor (IP) in the neighborhood of bearing #3, see Fig. 2. These plots are given as functions of time and relative to synchronous frequency domain. In this figure the lateral response is depicted in the form of journal bearing transverse displacement orbits and amplitude spectra of their time histories, where the gray lines correspond to the adjacent left-hand-side bearing #2 and the black lines correspond to the adjacent right-hand-side bearing #3. The torsional and axial responses are demonstrated by means of time histories and their amplitude spectra. Here, by the gray lines there are depicted, respectively, the responses registered at the bearing #1 and the shaft left-hand-side free end and by the black lines there are illustrated the responses registered at bearing #7 and the shaft right-hand-side free end, Fig. 2. In the case of such a crack the lateral response seems to be also har-

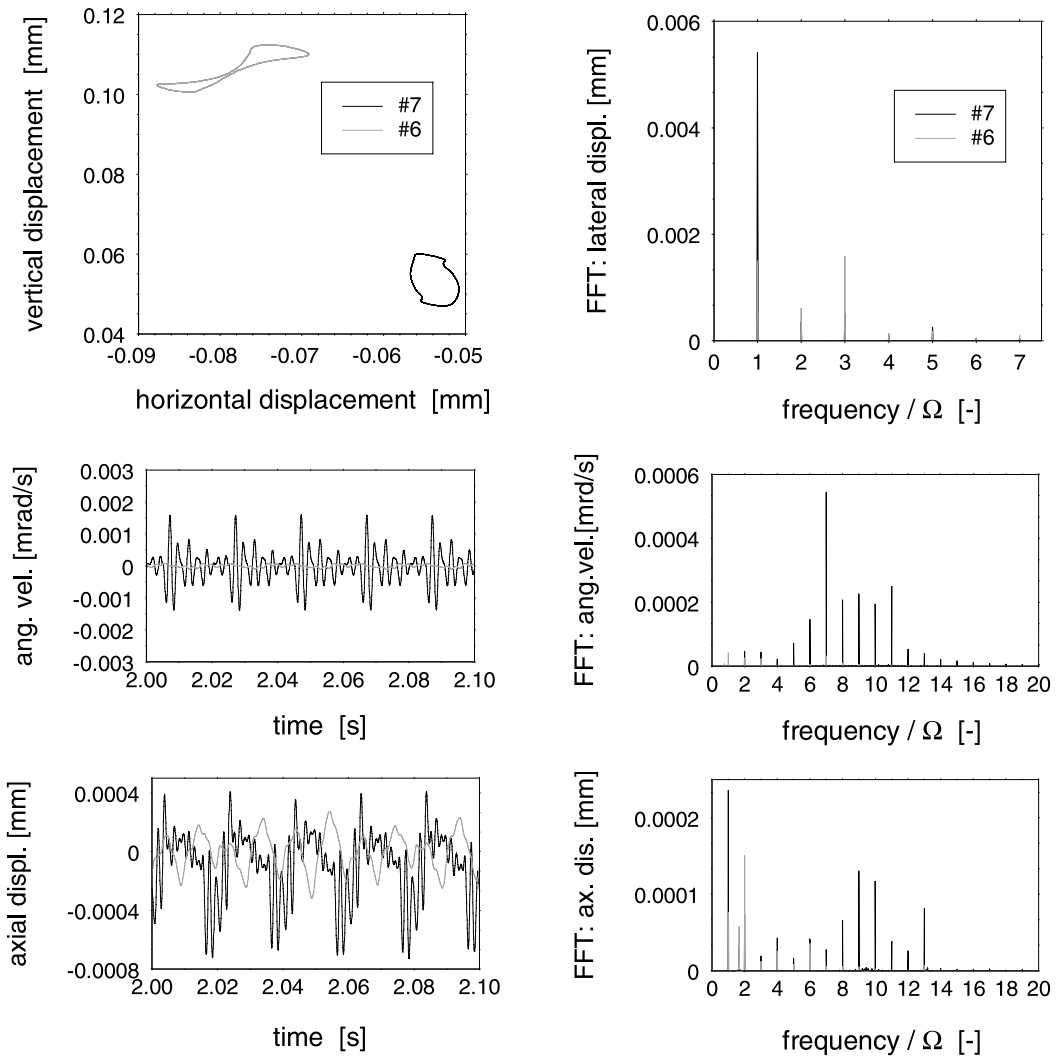

Fig. 7 Coupled dynamic response for the rotor-shaft system with the crack of the depth ratio $a/D = 0.25$ located at the generator-rotor mid-span

monic, which follows from the almost elliptical shaft displacement orbits plotted in Fig. 6. Here, although the respective bearing journal displacement orbits are still elliptical, but the amplitude spectra of their displacement time-histories are significantly affected by the double synchronous 2X and triple synchronous 3X frequency components. The torsional and axial responses are characterized by relatively severe extreme values for the monitoring devices operating on the real object. Their time histories are affected by many fluctuation components of relative frequencies 1X, 2X, 3X, 4X as well as by 7X÷13X in the case of the torsional response, and by almost all X multiplied frequencies (not all are visible in the presented scale) within 1X÷13X in the case of the axial response. Nevertheless, the highest peak of the axial response component corresponds to ∼1.66X approximately equal to the second axial natural frequency 83.044 Hz. In this case, the respective axial eigenform (presented in Fig. 5) is induced in the form of transient state component due to systematic closings and openings of the crack during each successive revolution of the shaft.

In the same way as in Fig. 6, in Fig. 7 there are presented results of analogous simulation obtained for a bigger crack of the depth ratio $a/D = 0.25$ and local-

ized in the generator rotor-shaft mid-span, i.e. in the cross section between bearings #6 and #7. Here, the lateral response is not harmonic. As it follows from Fig. 7, the bearing journal displacement orbits are not elliptical and the corresponding amplitude spectra of displacement time-histories are affected also by the remarkable frequency components 2X and 3X, in addition to the fundamental synchronous component 1X. In the case of the lateral response registered at bearing #6 the frequency component 3X is predominant which emphasizes the nonlinear-parametric character of the coupled dynamic response induced by this crack. The torsional response is also significant and the axial response is much more severe than that in the previous case. Nevertheless, in this case the ~ 1.66X transient state component of the axial response is much smaller in comparison with the remaining ones than in the previous example, which follows from the respective FFT-plots in Figs. 6 and 7.

It is noteworthy that torsional and axial responses obtained for various depth ratios within $a/D = 0.1 \div 0.3$ for the cracks located in several axial positions along the entire rotor-shaft line are characterized by similarly "rich" amplitude spectra as these obtained in the above examples, i.e. in general the same fluctuation components are excited with magnitudes rapidly increasing together with the crack a/D ratio. But mutual relations between the amplitude values of successive fluctuation components depend on particular cases of crack depths and locations. Similarly, the 2X and 3X frequency components of the system lateral response also significantly increase together with the rise of a/D, whereas maximum values of the peak corresponding to the synchronous 1X component remain almost unchanged.

According to the observed facts, as diagnostic parameters necessary for crack identification in the shaft, the maximum amplitude values of the 2X and 3X frequency components of the system lateral response as well as the resultant (global) amplitudes of the torsional and axial response have been selected. The mentioned resultant (global) amplitudes of the considered torsional and axial time histories are regarded here as maximum fluctuation values with respect to their average values of the steady-state dynamic response. The listed above values of response amplitudes corresponding to randomly generated crack parameters will constitute the database of numerical experiments used in the identification process.

5 Crack identification methods

The objective of the proposed methods is an efficient assessment of a possible damage of the vibrating rotor-shaft system when an information on system responses from monitoring devices is available. In addition to the identification of the most probable crack parameters, i.e. the crack location x_c and its depth a, the methods also provide a confidence measure of the results. Contrary to the method proposed by the authors in their previous paper [10], the methods described here consist of two major phases:

1. fast crack parameters identification based on the analysis of experimental data points generated before by the Monte Carlo sampling,
2. identification improvement strategy, mainly by enhancing the database in the neighborhood of the first phase estimation.

The second phase algorithms are meant to improve an accuracy of the identified crack parameters in a relatively short time, which is the time from the crack detection moment to the ultimate decision concerning the exploitation of the rotor machine. Moreover, these methods should enable us to use smaller databases reducing the costs of database preparation.

As it was mentioned, the foundation of all the presented methods is the database of points $(\mathbf{x}, \mathbf{y})$ relating the crack parameters $\mathbf{x}$ to the responses $\mathbf{y}$ of the vibrating rotor-shaft system (see Sect. 4). The database is created by means of the Monte Carlo sampling. A sample of crack parameters is generated according to the assumed probability distributions of the crack location x_c, the ratio a/D where D is the shaft diameter, and the circumferential crack position α_p. The choice of probability density functions (PDFs) was described in detail in [10]. In the identification example presented in the next section, 30% of the total number of sample points are generated using the uniform PDF in the range $a/D = 0.1 \div 0.4$ and the remaining points are generated using the following half-normal density function:

$$f(a) = \frac{2\vartheta}{\pi} \exp\left[-\frac{(a - a_{\min})^2 \vartheta^2}{\pi}\right], \tag{11}$$

where $a_{\min}$ is the minimal considered identifiable crack depth and ϑ is the parameter selected such that the probability of crack depth greater than the maximal

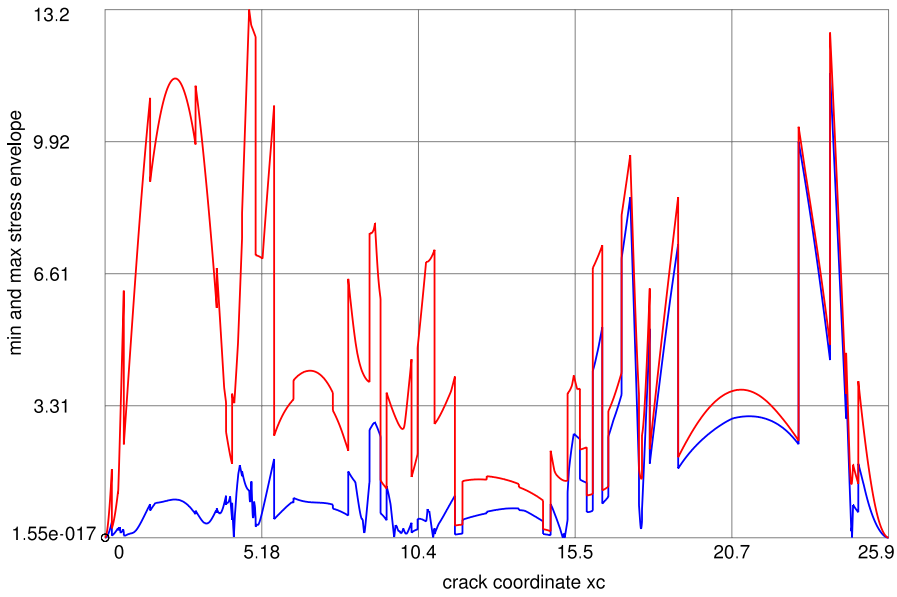

Fig. 8 Stress envelope for the uncracked rotor-shaft system supported on seven journal bearings

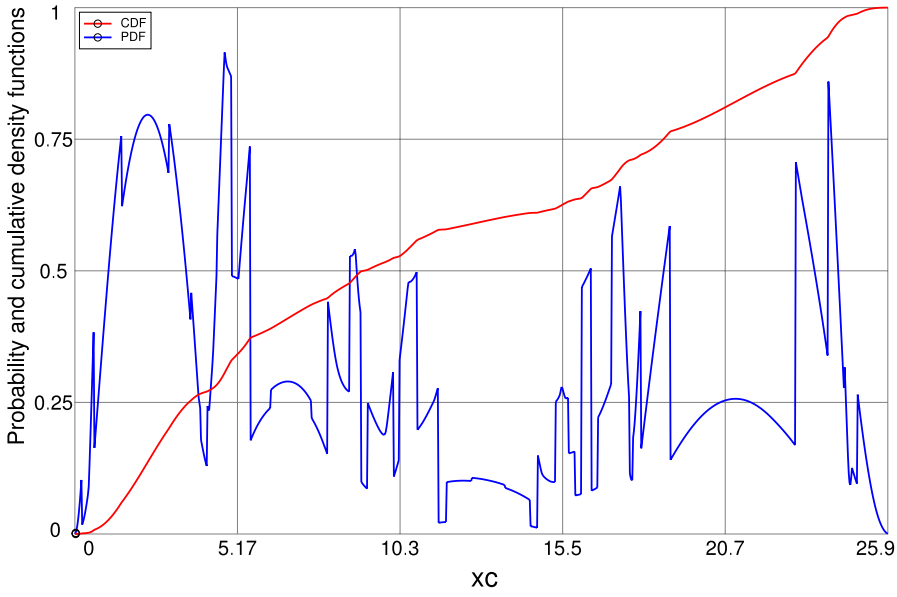

Fig. 9 Shape of the probability density function and the corresponding cumulative distribution function for the crack location x_c along the rotor-shaft system of the steam turbogenerator

depth observable in practice is negligible. In the case of PDF for the crack location x_c, it is taken to be proportional to the maximal reduced stress envelope obtained for the nominal uncracked rotor-shaft. Such an envelope for the considered rotor-shaft system shown in Fig. 2 is presented in Fig. 8. The PDF corresponding to the stress envelope can be expressed as

$$f(x_c) = \frac{|\sigma(x_c)|}{\int_{x_1}^{x_7} |\sigma(x)|\,\mathrm{d}x}, \quad x_c \in [x_1, x_7] \tag{12}$$

where $\sigma(x)$ is the maximal reduced stress function and x_1 and x_7 are the axial coordinates of the first and the seventh bearing, respectively (see Fig. 9 for PDF and the corresponding cumulative distribution function (CDF)). Similarly to the case of crack depth, 30% of the total number of points are generated from the uniform PDF in the range $[x_1, x_7]$ and the remaining sample points are drawn using the PDF (12) to add numerical experiments at locations where cracks are most likely to occur.

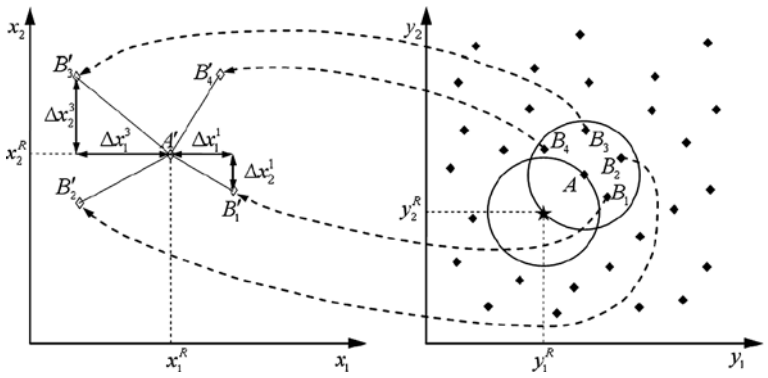

Fig. 10 Illustration of the identification algorithm

One of the major advantages of one-dimensional hybrid dynamical models of the rotor-shaft systems is their high computational efficiency. A single analysis of the parametric-nonlinear coupled vibration process usually takes less than 75 seconds of CPU on modern PCs. Hence, accounting for inherent parallelism of the Monte Carlo method, in most of the cases it is affordable to perform hundreds of thousands or even millions of simulations. This allows for thorough exploration of the response space, which facilitates the identification process. Nevertheless, still the number of sample points (size of the database) should be large enough to ensure acceptable identification accuracy.

Below, there are presented the "reference" identification algorithm, named here the nearest-point method, and three second-phase algorithms for improvement of the results obtained using the nearest point method. A confidence/tolerance measure for the identified parameters is also described.

Nearest-point identification method (NP) Crack parameter identification in the nearest-point identification method consists in localizing a point in the space of responses of the rotor-shaft system that is the closest to the read-out from a monitoring device. The accuracy of the NP method increases together with the database size. Therefore, the largest possible databases have to be used, cf. [10] where this method is described in detail. Unquestionable advantage of this approach is almost immediate identification of crack parameter values as well as their tolerances.

The NP method can be schematically presented in two-dimensional space of parameters x_1 and x_2 and the corresponding space of two responses y_1 and y_2, see Fig. 10. In this figure, the read-out (y_1^R, y_2^R) is marked with the star and the diamond markers depict sample points—the responses for randomly generated parameters. In Fig. 10, the point in the response space, which minimizes the distance from the read-out, is point A. The coordinates (x_1^R, x_2^R) of point A', corresponding to A in the parameter space, are assumed as identification results, i.e. the parameters leading to the read-out. Such identification results are biased. They very much depend on the database size as well as on a local "saturation" of the responses space with the sample points. Therefore, some measure of confidence for identification results should also be provided. The confidence measure introduced in [10] is briefly described below.

In the response space, there are points B_i, $i = 1, \ldots, N_A$, falling into the spherical vicinity of the point A of the radius equal to the distance between A and the read-out. We also identify N_A points B'_i in the parameter space that are mapped onto B_i points. If there are no points in the spherical vicinity, its radius is gradually enlarged until at least two points are inside. For each point B'_i the differences $\Delta x_j^i = |x_j^R - x_j^i|$ are computed, where x_j^i is the jth coordinate of the point B'_i, $j = 1, \ldots, n$, n being the number of parameters, $n = 2$ here. A conservative tolerances for the identified parameters x_j^R can be then defined using the computed differences as

$$\hat{x}_j^R = \max_{i=1,\ldots,N_A} \Delta x_j^i, \tag{13}$$

and the identification results given as $x_j^R \pm \hat{x}_j^R$. The described confidence measure is the same for all the identification methods presented in this section.

The nearest-point identification approach is rather straightforward. It is particularly well suited for rotor-shaft damage identification where, owing to computa-

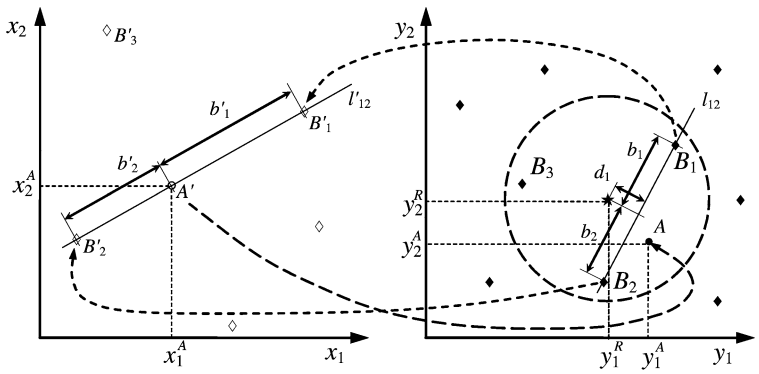

Fig. 11 The idea of orthogonal projection identification method

tionally efficient models of rotor-shaft systems, very large samples can be afforded.

Orthogonal projection identification method (OP) The idea of orthogonal projection method is illustrated in Fig. 11. Similarly as in Fig. 10, here the read-out is marked with the star and the diamond markers denote sample points, i.e. they are the responses for randomly generated crack parameters. The OP algorithm starts by searching for the pair of points in the read-out vicinity, which define the straight line that is closest to the read-out. In Fig. 11 these are points are B_1 and B_2 and the line is denoted as l_{12}. Next, the read-out is projected on l_{12} determining two segments b_1 and b_2 connecting the projection point with B_1 and B_2, respectively. In the parameter space the points corresponding to B_1 and B_2 are B'_1 and B'_2, respectively, and the straight line passing through these points is denoted l'_{12}. Accounting for the proportion b_1/b_2 and the position of the projection point with respect to B_1 and B_2, point A' is established on l'_{12} as an approximation of the projection point mapping. Then, at this point the vibrating rotor-shaft system responses are computed yielding point A with coordinates (y_1^A, y_2^A). This point is added to the database and the procedure restarts. If point A is localized in the vicinity of the read-out, it will probably be used in the next iteration as one of the points constituting the closest straight line. In turn, it is likely to produce a new A point that is closer to the read-out than the previous A point. If this is not the case, the procedure is stopped. Another stop criterion may be set on the number of iterations. The parameter values corresponding to the best A point (provided it is closer to the read-out than any of the original database points) are taken to be the identification results.

The main advantage of the OP method is a small number of additional simulations of the rotor-shaft dynamic responses. However, due to strongly nonlinear character of the considered relationship there is no guarantee that the methodology will always improve the NP identification results.

Nedler–Mead identification method (NM) This nonlinear simplex method is a popular direct search optimization technique introduced by Nedler and Mead, see [11], that has been adopted to the considered identification problem. The simplex graph based on the set of $n + 1$ points in the parameter space, n being the number of parameters, corresponding to $n + 1$ points closest to the read-out in the response space is employed. Each time during the optimization process a new point (values of crack parameters $\mathbf{x}$) is established the appropriate rotor-shaft responses $\mathbf{y}$ are computed and the new point is added to the database. The objective function that is to be minimized here is the distance in the response space between the read-out and the closest database point. The procedure is stopped if the minimized distance is smaller than certain ε tolerance or the number of calls to the rotor-shaft simulation program is exceeded.

Similarly to the OP method, the NM identification algorithm requires some additional simulations of the rotor-shaft system dynamic responses, which increase the identification time. However, this additional computational effort can be controlled in a quite flexible way depending on the user preferences. In terms of the distance from the read-out the method always results with a solution, which is not worse than the NP-based identification.

Local sampling identification method (LS) The LS method seems to be the simplest choice for improv-

ing the accuracy of the NP identification results. The method consists in finding the two closest points $\mathbf{y}_A$ and $\mathbf{y}_B$ to the read-out $\mathbf{y}^R$ and computing the system responses for a certain number of new points sampled in the crack parameter space using PDFs determined in some way by $\mathbf{y}_A$ and $\mathbf{y}_B$. These new points are generated from the independent uniform distributions, where point $\mathbf{x}_A$ (related to the closest point $\mathbf{y}_A$) is the mean vector and the absolute differences between the respective parameter values of $\mathbf{x}_A$ and $\mathbf{x}_B$ are the standard deviations of the assumed distributions.

In the numerical example that follows the identification capacity of the proposed methods is tested for the turbogenerator rotor-shaft system described in Sect. 4. For randomly generated cracks (given by the parameters x_c, a/D and α_p) the system responses are first computed using the one-dimensional hybrid model and then, at the second step, the obtained results are introduced as read-outs to the identification algorithm indicating the most probable crack parameters. A comparison of the identified parameters and the original ones provides a measure of the identification quality.

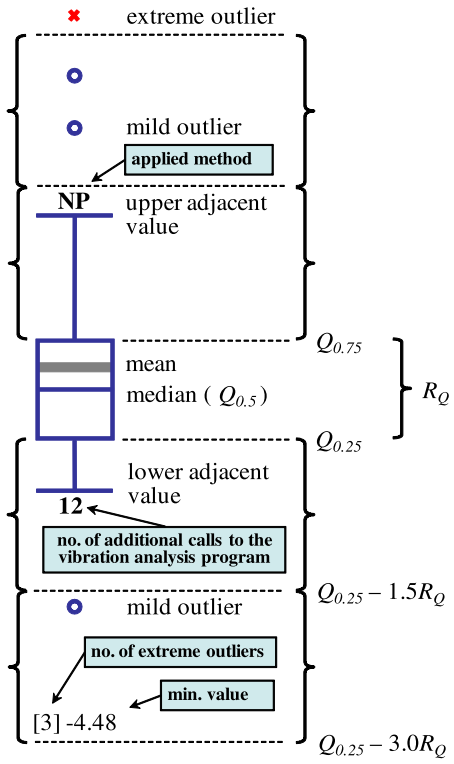

Fig. 12 Box plot notation

6 Numerical example, identification analysis of the rotor-shaft system of the steam turbogenerator

The effectiveness of the crack parameters identification methods described in Sect. 5 is compared using the hybrid mechanical model of the steam turbogenerator rotor-shaft system supported on seven journal bearings shown in Fig. 2. Selected statistics for all the methods and for database sizes of 5,000, 10,000, 50,000, 100,000, 200,000 and 500,000 points, respectively, as well as the average computational effort have been collected in one diagram, a so-called *box plot*. The box plot consists of the following statistics, see Fig. 12: the lower adjacent value (non-outlier simulation), the lower quartile $Q_{0.25}$, the median, the mean value, the upper quartile $Q_{0.75}$ and the upper adjacent value (non-outlier simulation). Moreover, the box plot depicts simulations considered unusual, called outliers, which are smaller than $Q_{0.25} - 1.5R_Q$ or grater than $Q_{0.75} + 1.5R_Q$, where $R_Q = Q_{0.75} - Q_{0.25}$ is the interquartile range. The outliers are divided into two groups: *mild* outliers (marked with navy blue circles)—simulations not smaller than $Q_{0.25} - 3.0R_Q$ or not grater than $Q_{0.75} + 3.0R_Q$, and *extreme* outliers (marked with the red crosses)—which are farther than the mild ones. For the sake of presentation quality, not always all the extreme outliers are shown. When this is the case, the number of hidden extreme outliers (in the brackets) and the maximal/minimal values are specified.

Each of the box plots presented below displays identification statistics for 100 tests. The box plots are prepared for the identification error of two crack parameters: x_c and a/D, and their identification tolerances.

As it can be expected, the identification results for x_c strongly depend on the database size. Irrespective of the identification approach, the smallest databases of 5,000 or even 10,000 simulations do not provide a good identification quality and the obtained results are far from being reliable, see Fig. 13. All the methods produce many extreme outliers; moreover, the difference between the lower adjacent value and the upper adjacent value vary in quite a wide range of 0.7–1.4 m related to the entire rotor-shaft length of 25.9 m. Slightly better identification results are pro-

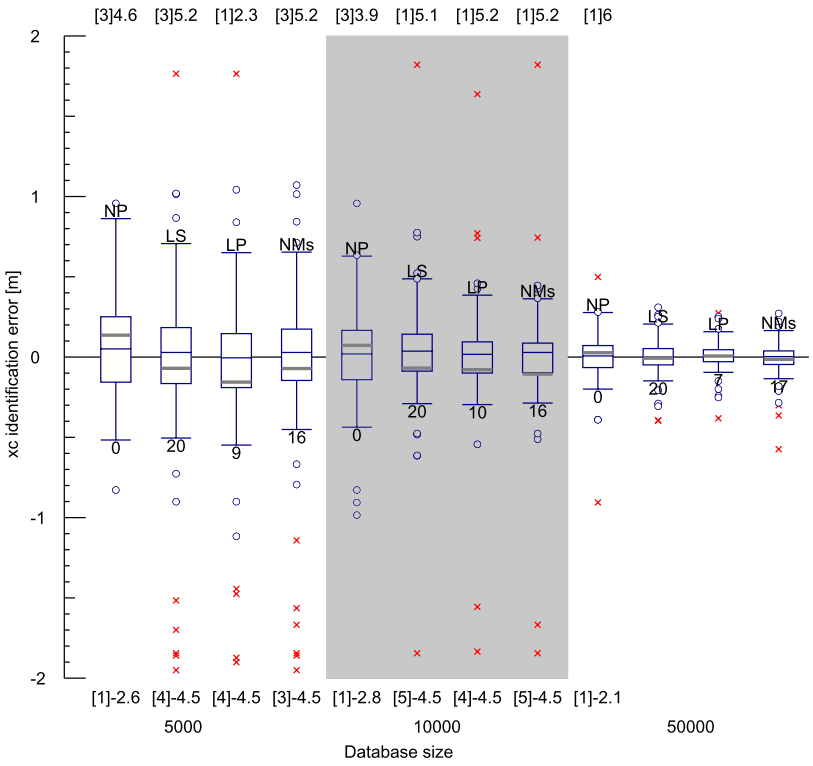

Fig. 13 Box plots of x_c identification error for database sizes equal to 5,000, 10,000 and 50,000, respectively

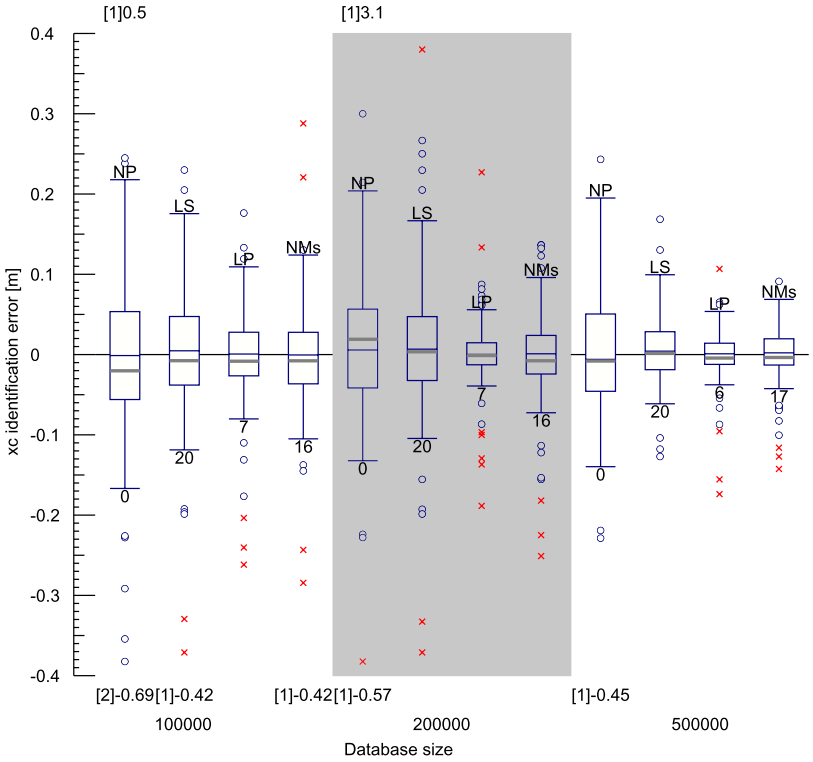

Fig. 14 Box plots of x_c identification error for database sizes equal to 100,000, 200,000 and 500,000, respectively

duced when the database of 50,000 points is used. Unfortunately, even in this case, some extreme outliers can be observed. There are two tests for the NP identification method that completely failed resulting with identification errors of up to 6 m. Therefore, the fast NP method alone is not sufficiently reliable for such a medium size database and some improvement algorithm needs to be employed.

More promising results deliver identification tests corresponding to large databases of 100,000, 200,000 and 500,000 simulations, see Fig. 14. Here, the NP method for all the three cases has almost the same scatter which can be considered as acceptable. The only extreme outlier, registered in an identification test performed with 200,000 points database spoils a little generally very good accuracy and concentration of the results. Unquestionably, the best results for all the examined methods are obtained using the largest database (500,000 data points), which only proves the intuitive relationship between the database size and identification accuracy. However, also with databases of 100,000 and 200,000 points one may obtain reliable and accurate results, especially when it is possible to use one of the improving algorithms, the OP, NM or LS. The fastest and the most successful among them seems to be the OP method, which needs only about 7 additional simulations.

Identification tolerances of x_c for small databases confirm a poor quality of the results obtained by all the methods, see Fig. 15. The only exception is the OP identification method with the database of 50,000 points where the largest computed tolerance does not exceed 0.45 m. The quality of OP is not much improved for databases of 100,000 and 200,000 points, Fig. 16. However, significant improvement is observed for the largest database, where the outermost value of extreme outlier is approximately 0.13 m, and other statistics are better than for the remaining methods.

Similar tolerance statistics are computed only for the NM method. However, about 16 additional simulations have to be done compared to 7 for OP. It should be noticed that the NP method possesses good tolerance statistics in the case of the two largest databases. Nevertheless, in the considered example only the largest database enables us to obtain reliable and accurate results. By this we assume identification of the crack position in the monitored rotor-shaft of the total length of 25.9 m with the maximum error equal to 0.7 m (the most likely maximum error equals to 0.5 m) and the maximum tolerance equal to 0.45 m (the most likely maximum tolerance is 0.3 m) in the worst case.

At the same time, in the case of x_c, the considered identification improvement methods give comparable results, the maximum error smaller than 0.2 m and the maximum tolerance smaller than 0.15 m for the NM and OP methods.

The identification process of a/D ratio yields bigger scatter of identification results, i.e. every applied database and considered method have many mild and extreme outliers, see Figs. 17–20. As in the case of the parameter x_c, the scatter magnitude decreases together with the increase of database size, which enables us to choose an appropriate level of accuracy sufficient for monitoring and improvement of identification results. In the case of the largest database the NP method yields the maximum identification error equal to 0.065 m, which is about 15% of the assumed a/D value. Slightly better results can be observed for the improvement algorithms NM and LS. The maximum identification error they produce is 0.04 m, which is not more than 10% of the maximum assumed a/D. The most efficient in a/D identification improvement seems to be the OP method, both in terms of accuracy and computational time.

7 Conclusions

In the present paper, nonlinear and parametric components of coupled bending–torsional–axial vibrations have been used as a transverse crack occurrence symptoms in rotor-shafts of the rotor machines. For this purpose, by means of the structural hybrid model of the real object, several databases containing results of dynamic responses corresponding to various possible crack depths and locations on the shaft were generated using the Monte Carlo simulation. Special probability density functions of crack parameters were proposed in order to ensure good identification quality for the most probable crack parameters. In order to detect and localize the crack, four identification methods have been applied and mutually compared. These are: the nearest-point method (NP), the orthogonal projection method (OP), the Nedler–Mead method (NM) and the local sample method (LS). Each of them was tested from the viewpoint of computational efficiency and crack identification error on the example of the rotor-shaft system of large steam turbogenerator.

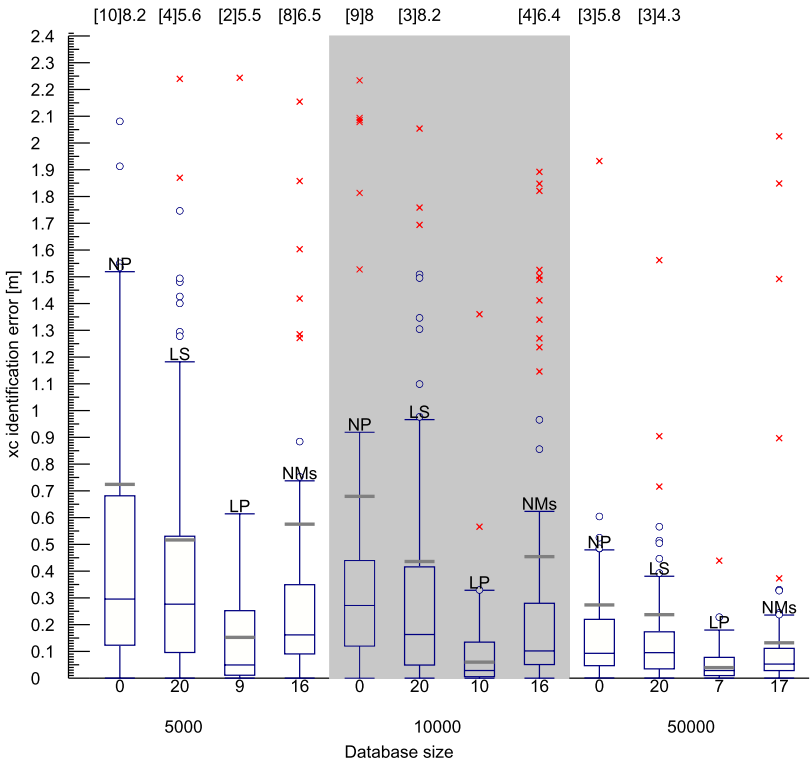

Fig. 15 Box plots of x_c identification tolerance for database sizes equal to 5,000, 10,000 and 50,000, respectively

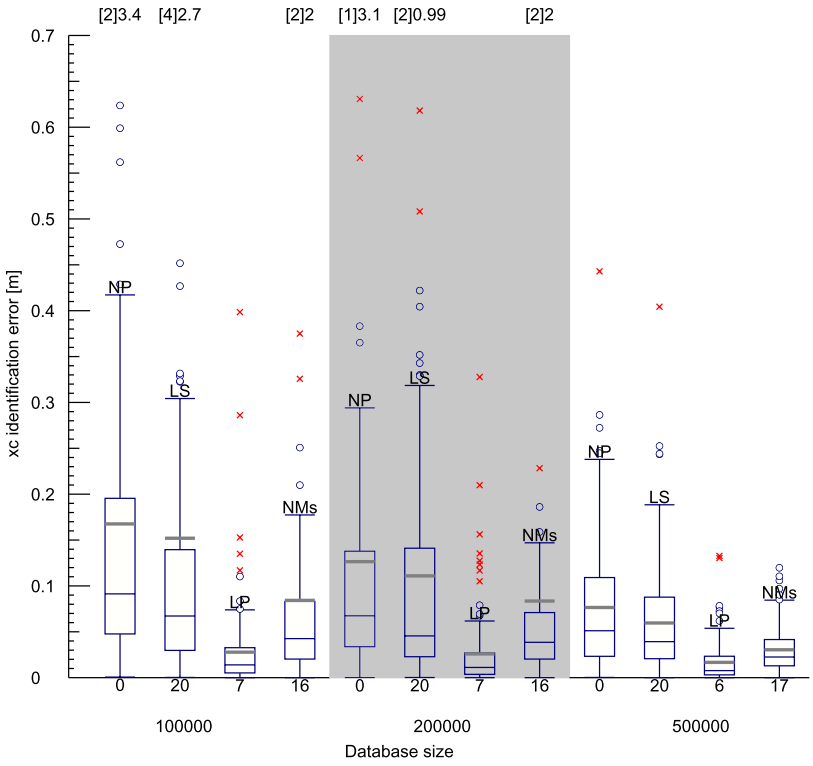

Fig. 16 Box plots of x_c identification tolerance for database sizes equal to 100,000, 200,000 and 500,000, respectively

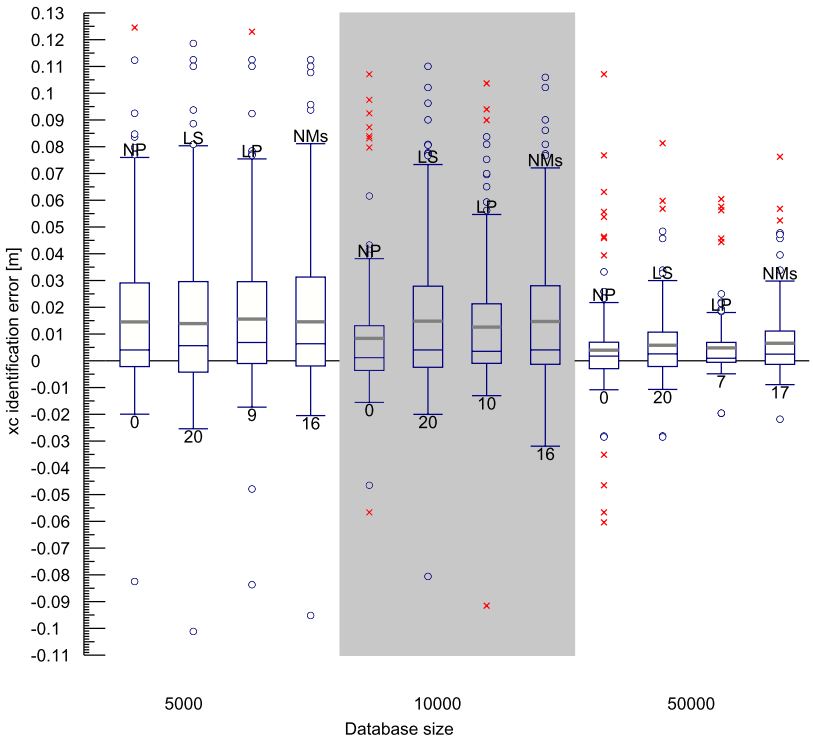

Fig. 17 Box plots for a/D identification error for database sizes equal to 5,000, 10,000 and 50,000, respectively

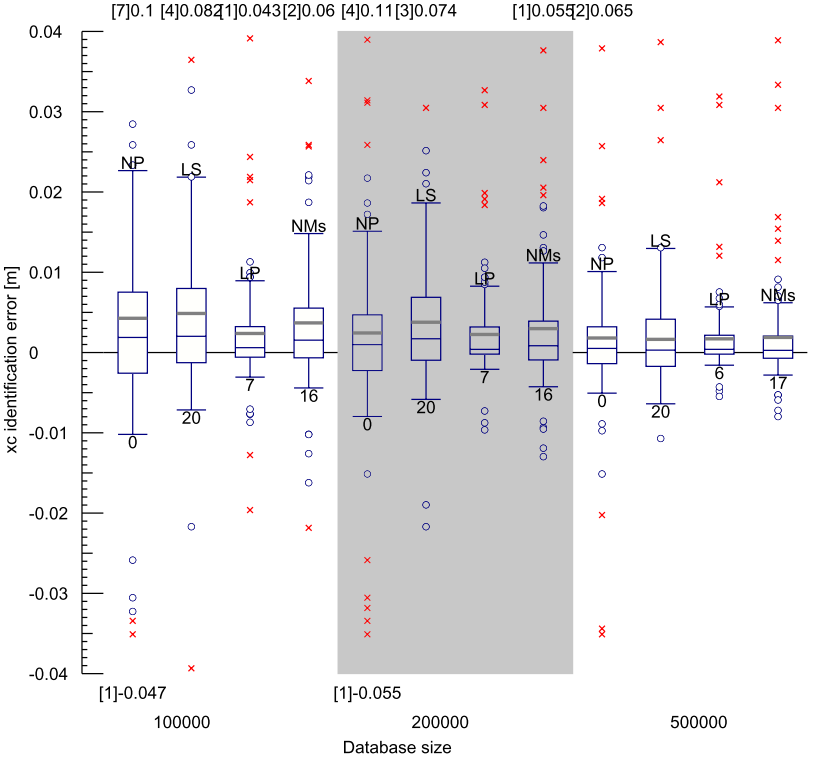

Fig. 18 Box plots of a/D identification error for database sizes equal to 100,000, 200,000 and 500,000, respectively

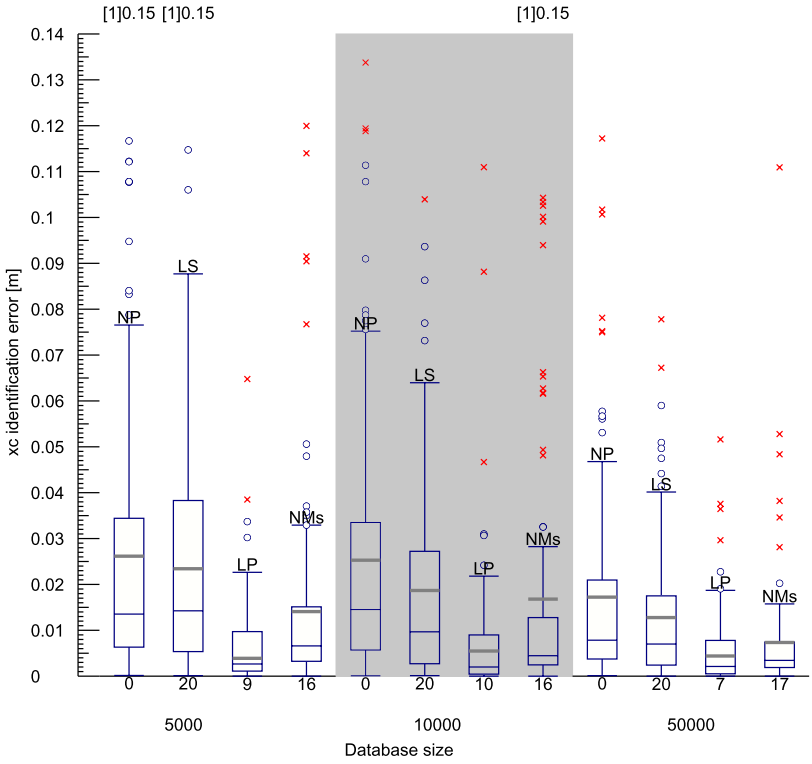

Fig. 19 Box plots of a/D identification tolerance for database sizes equal to 5,000, 10,000 and 50,000, respectively

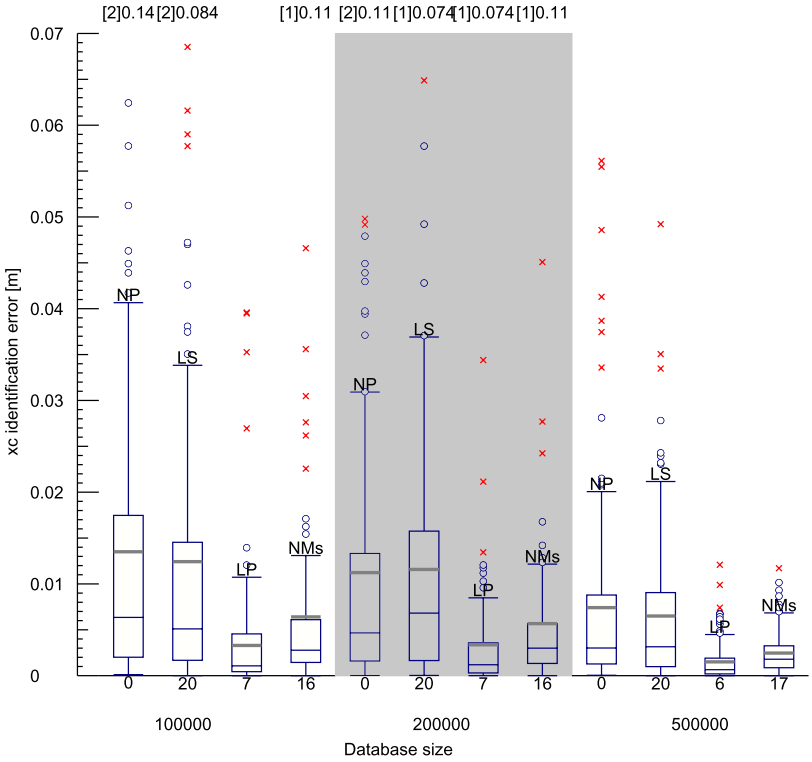

Fig. 20 Box plots of a/D identification tolerance for database sizes equal to 100,000, 200,000 and 500,000, respectively

From the carried out considerations it follows that the Monte Carlo sampling approach for damage identification in vibrating rotor-shaft systems, together with the proposed methods of improving the accuracy of results, seems to be an appropriate solution for industrial engineering applications. The crucial advantage of the proposed procedure is the immediate identification process of the real rotor-shaft system under on-line monitoring. The method is based on the previously prepared database of hundreds of thousands numerical experiments, that takes significant but still acceptable computational effort proportional to the demanded accuracy of the results. Additionally, the same database can be used to obtain in relatively short time (5 to 20 minutes on a present-day PC) more precise estimation of the crack parameters. The identification error scatter and the scatter of tolerance decrease with the database size, which allows to obtain required accuracy of crack parameter identification. Based on the test results the identification improvement method that seems to be the most efficient and accurate is the orthogonal projection identification method (OP).

Acknowledgements The partial support from the Polish Committee for Scientific Research grants PBZ-KBN-105/T10/2003, No. N519 010 31/1601 and No. 3T11F00930, is gratefully acknowledged.

References

1. Zhao, M., Luo, Z.H.: A convenient method for diagnosis of shafting crack. In: Proc. of the 12th Biennial ASME Conference on Mechanical Vibration and Noise. ASME, Rotating Machinery Dynamics, DE-Vol. 18-1, pp. 29–34. Montreal, Canada (1989)
2. Ishida, Y., Yamamoto, T., Hirokawa, K.: Vibrations of a rotating shaft containing a transverse crack (major critical speed of a horizontal shaft). In: Vibration Institute (eds.), Proc. of the 4th Int. IFToMM Conf. on Rotor Dynamics, pp. 47–52. Chicago, Willowbrook, IL, Sept. (1994)
3. Kiciński, J.: Dynamics of rotors and journal bearings. In: Institute of Fluid-Flow Machinery of the Polish Academy of Sciences (eds.), Fluid-Flow Machinery, p. 28. Gdańsk (in Polish) (2005)
4. Pennacchi, P., Bachschmid, N.: A model-based identification method of transverse cracks in rotating shafts suitable for industrial machines. Mech. Syst. Signal Process **20**, 2112–2147 (2006)
5. Darpe, A.K., Gupta, K., Chawla, A.: Coupled bending, longitudinal and torsional vibrations of a cracked rotor. J. Sound Vib. **269**, 33–60 (2004)
6. Szolc, T., Bednarek, T., Marczewska, I., Marczewski, A., Sosnowski, W.: Fatigue analysis of the cracked rotor by means of the one- and three-dimensional dynamical model. In: Proc. of the 7th International Conference on Rotor Dynamics. Organized by the IFToMM in Vienna, Sept., Austria, Paper-ID 241 (2006)
7. Papadopoulos, C.A., Dimarogonas, A.D.: Coupling of bending and torsional vibration of a cracked Timoshenko shaft. Ingenieur-Archiv **57**, 257–266 (1987)
8. Ostachowicz, W., Krawczuk, M.: Coupled torsional and bending vibrations of a rotor with an open crack. Arch. Appl. Mech. **62**, 191–201 (1992)
9. Szolc, T.: On the discrete-continuous modeling of rotor systems for the analysis of coupled lateral-torsional vibrations. Int. J. Rotating Mach. **6**(2), 135–149 (2000)
10. Szolc, T., Tauzowski, P., Stocki, R., Knabel, J.: Damage identification in vibrating rotor-shaft systems by efficient sampling approach. Mech. Syst. Signal Process. (2008, in press)
11. Nedler, J.A., Mead, R.: Simplex method for function minimization. Comput. J. **7**, 308–313 (1965)